Prediction of carbon dioxide dissolution in bulk water under isothermal pressure decay at different boundary conditions

Yasin Gholami [a], Reza Azin [a], Rouhollah Fatehi [b], Shahriar Osfouri [c], Alireza Bahadori [d,*]

[a] Department of Petroleum Engineering, Faculty of Petroleum, Gas, and Petrochemical Engineering, Persian Gulf University, Bushehr, Iran
[b] Department of Mechanical Engineering, Faculty of Engineering, Persian Gulf University, Bushehr, Iran
[c] Department of Chemical Engineering, Faculty of Petroleum, Gas, and Petrochemical Engineering, Persian Gulf University, Bushehr, Iran
[d] School of Environment, Science and Engineering, Southern Cross University, Lismore NSW, Australia

ARTICLE INFO

ABSTRACT

In this work, dissolution of CO_2 in bulk water is simulated under isothermal pressure decay. Different boundary conditions (BCs) including equilibrium, semi-equilibrium and non-equilibrium are examined at gas/liquid interface. Comparison of our simulated and measured experimental data shows that the non-equilibrium BC can predict dissolution behavior reliably. Other boundary conditions show considerable deviation between model predictions and experimental measurements. On the other side, convective dissolution is found much more active than diffusive mixing, so that the role of diffusive transport is overshadowed. Mass transfer coefficient is highest at the start of dissolution and decreases with time. Results show that when convection is the active mechanism even at late times, it interferes with diffusivity measurements and makes interpretation of diffusion experiment results difficult both at early and later times.

© 2014 Elsevier B.V. All rights reserved.

1. Introduction

Transfer of gases, tracers, and concentrated species into solvents is controlled by the mechanisms of mass transfers i.e. convection and diffusion. For a system like CO_2 and water, as CO_2 is dissolved in water, a heavier layer forms at an interface and causes CO_2 to dissolve rapidly in the form of instabilities. This process has a direct application in CO_2 geological storage where free phase gas is dissolved in brine after a long time. Modeling of miscible gas injection in all types of crude oil is analogous to CO_2 injection.

The main difference in modeling such processes refers to the presence of convection [1], liquid swelling [2], solubility [3], and dependence of parameters (such as diffusivity, viscosity) on pressure or temperature or time [4,5]. As it is mentioned, when CO_2 dissolves in water, heavier water saturated with CO_2 at the interface tends to sink down the water column by making instabilities.

The similar steady-state problem in heat transfer is known as Rayleigh–Bénard convection in which fluid is confined between two parallel horizontal plates with hot fluid rising and cold fluid falling [6]. In our study, CO_2 concentrated water is falling due to gravity effect while fresh water rising to reach an equilibrium state in CO_2-saturated water. Thus, the same criteria of the Rayleigh–Bénard convection can be used for our study by using the analogy. However, due to differences in boundary conditions and time conditions, results can be expected different.

Modeling instabilities caused by density difference has been considered for a long time. The works of Rayleigh and Taylor on modeling instability stand out as the problem named after them [7,8]. After that, many works tried to model, simulate and perform the experimental design of Hele-Shaw [9], Rayleigh–Bénard [10,11], Rayleigh–Taylor and Saffman–Taylor [12] problems.

However, few works can be cited to discuss instability growing for two miscible phases when one phase dissolves from the interface.

In this study, numerical and experimental dissolution of CO_2 in water is evaluated under pressure decay. The dissolution sequences are distinguished based on the trend of the Sherwood number like Hassanzadeh et al. [13]. However, our discussion includes dissolution in both porous media and bulk water. Many other works can be referred that modeled or simulated convective dissolution in porous media for reservoir applications such as Ghesmat et al. [14], Ouakad and Nasrabadi [15] and Szulczewski et al. [16].

While, experimental applications imply simulation of convective mixing in bulk fluid which is the main topic of our work. Farajzadeh et al. [17] simulated CO_2 dissolution in bulk water in axisymmetric coordination. They used equilibrium boundary condition (BC) at the interface and observed instabilities in the form of Rayleigh–Taylor problem.

Although, more perturbed results are expected. In another work, Haugen and Firoozabadi [18] studied the effect of bulk flow due to non-ideality and compressibility on dissolution. They showed that neglecting bulk flow results in fitting of Fick's second law with higher diffusion

coefficients. We know that natural density-driven convective flux is much more significant than the so-called mechanisms of non-ideality or compressibility addressed in the work of Haugen and Firoozabadi [18].

Another criterion for modeling the gas dissolution is choosing the proper boundary condition at gas/liquid interface. In literature, different boundary conditions are used for modeling. Most works considered a saturated interface i.e. equilibrium or semi-equilibrium BC [19–22].

Recently some authors have considered other forms of boundary conditions rather than simple equilibrium BC [23–25]. They used a Neumann boundary condition type at gas/liquid interface accounting for the effect of declining pressure versus time. Non-equilibrium BC is another form of boundary condition standing for the effect of interface resistance.

The pioneer works of Civan and Rasmussen [2,3,26] illustrates this BC. However, a more general form is described by Etminal et al. [27] in which a sharp concentration change across the interface is considered. In the following sections, we first explain experimental procedure briefly and then present our assumptions, equations and boundary conditions.

After that, convective dissolution of CO_2 in water under pressure decay is modeled. We used the experimental data obtained from a PVT cell and the data of Rongy et al. [28] to see validity of our model. Concluding remarks appear at the end of the paper.

2. Material and methods

A PVT cell is filled with liquid (water) sample up to a special height (H) (see Fig. 1). Details of experimental setup used here were described by Azin et al. [29] in which a certain amount of gas is brought into contact with water and pressure is recorded as gas is dissolving in water.
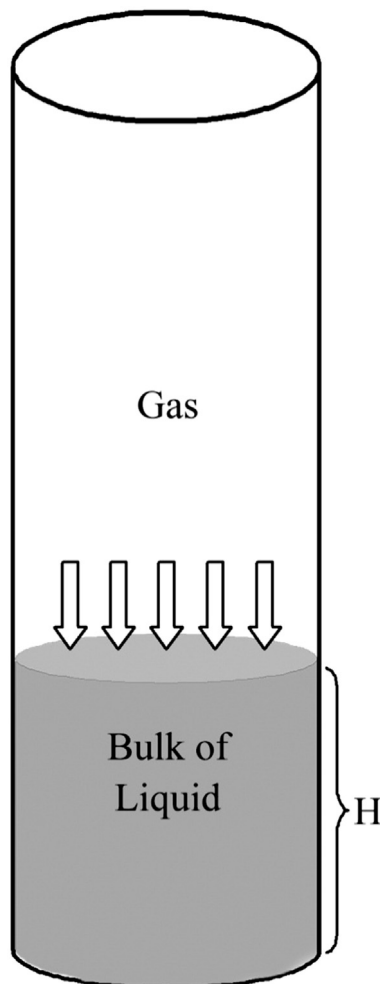

Fig. 1. A PVT cell shows the initial state of fluids for conducting a pressure decay test.

The same approach is used by many authors to calculate diffusion coefficient in oil as an inverse problem based on Fick's second law of diffusion [19,21,30,31]. The cell is mounted under the injection line and gas is injected from top of the cell. The gas injection process continues to reach the required initial pressure.

Then, the injection line is shut off and the test starts by recording pressure versus time periodically. The whole cell is put through a thermal air bath to keep the temperature constant. All the connecting valves are tested frequently to prevent any leakage. The tests are conducted until a steady pressure is reached.

The steady pressure is the same as the equilibrium pressure. Depending on the method of diffusivity calculation, this equilibrium pressure can have significant effect on the results. The high pressure cell has inner dimensions of 3.81 cm in diameter and 31 cm in height. The CO_2 gas cylinder was obtained from domestic suppliers and has 99.99% purity. Distillated water was provided from a generator in the chemistry laboratory, which filled 10 cm height of high pressure cell.

3. Mathematical modeling

Mathematical modeling is based on the experimental conditions. Our modeling uses the following assumptions:

1. There is no chemical reaction in the system.
2. Two dimensional and Cartesian coordinate describe our geometry.
3. Evaporation of water into the gas phase is negligible [17,32].
4. Resistance of mass transfer at water/CO_2 interface can be neglected (Equilibrium or Semi-equilibrium boundary condition) or considered (Non-equilibrium boundary condition).
5. There is no pressure gradient in the CO_2 phase [32].
6. Swelling of water due to dissolution of CO_2 is negligible [29]. Thus, interface position during the run is constant [32,33].
7. Due to low solubility of CO_2 in water (compared to CO_2 in hydrocarbons) diffusion coefficient versus time and position is assumed to be constant.
8. The whole process is isothermal.
9. Viscosity of water does not change due to CO_2 dissolution.
10. Boussinesq approximation is valid.

Assumptions 5 and 6 imply that the geometry is a regular rectangle with the diameter and height of high pressure cell filled with water. Fig. 2 shows a schematic of the model geometry. It should be added that however experiments are conducted in a cylindrical PVT diffusion cell, a Cartesian geometry is used here. Axisymmetric coordinates result in symmetric fingers which are not of interest. The similar problem is modeled in a 2-D Cartesian geometry by Rongy et al. [28].

From the real gas law, the number of CO_2 gaseous moles at a specified pressure can be calculated:

$$PV = znRT \Rightarrow n_g = \frac{PV_g}{ZRT}. \tag{1}$$

Pressure change among the runs is not that much (<5% of the initial pressure) to use more complicated equation of states. The prescribed equation will be used for conversion between gas pressure and aqueous CO_2 concentration, which is a simple linear relationship. Assuming that gas compressibility factor is constant as pressure decays, the difference between initial and current gaseous CO_2 can be written:

$$\Delta n_g = \frac{\Delta P V_g}{ZRT}. \tag{2}$$

The change in CO_2 moles can be written in terms of the average concentration in bulk liquid, $\bar{c}_{CO_2} \left(\frac{mol}{m^3} \right)$:

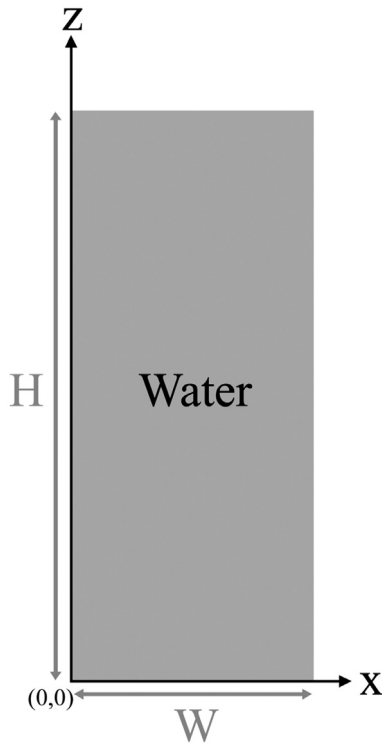$$\Delta n = -V_l \Delta \bar{c}_{CO_2}. \tag{3}$$

Fig. 2. The geometry used in dissolution modeling, which considers the water column only.

The difference between initial mole of gas and the gaseous mole remaining in the cell is equal to dissolved CO_2. Thus, Eq. (2) is equal to Eq. (3) and pressure can be obtained:

$$\frac{\Delta P V_g}{ZRT} = -V_l \Delta \bar{c}_{CO_2} \Rightarrow \Delta P = \frac{-V_l ZRT \Delta \bar{c}_{CO_2}}{V_g}. \tag{4}$$

As a result, gas pressure can be calculated from the following equation:

$$P = \frac{-V_l ZRT \bar{c}_{CO_2}}{V_g} + P_i. \tag{5}$$

Wherever pressure is given, CO_2 average concentration can be calculated from Eq. (5), and vice versa. In our numerical solution pressure is calculated from the above equation. When equilibrium pressure is known, the above equation can be rewritten as:

$$P_{eq} = \frac{-V_l ZRT \bar{c}_{eq,CO_2}}{V_g} + P_i. \tag{6}$$

Table 1
Boundary conditions for Eq. (9).

Condition	Type	Eq.
$t = 0$	Initial condition	$u = v = 0$
$x = 0$	Impermeable wall	$u = v = 0$
$x = l$	Impermeable wall	$u = v = 0$
$z = 0$	Impermeable wall	$u = v = 0$
$z = H$	No flow	$v = 0$

Table 2
Boundary and initial conditions for Eq. (10).

Condition	Type	Eq.
$t = 0$	–	$c = 0$
$x = 0$	Impermeable wall	$\nabla c = 0$
$x = l$	Impermeable wall	$\nabla c = 0$
$z = 0$	Impermeable wall	$\nabla c = 0$
$z = H$	Dirichlet, time-dependent	$c = c_{sat}(P_i)$
	Dirichlet, Robin	$c = A\bar{c}(P) + B$
		$D\frac{\partial c}{\partial z}]_{z=H} = k(c_{g\text{-}int}(t) - c_{sat}(P))$

Thus, $\bar{c}_{eq,CO_2}$ which is solubility of CO_2 in water at the required pressure, can be calculated by rearranging the above formula:

$$\bar{c}_{eq,CO_2} = \frac{V_g\left(P_i - P_{eq}\right)}{V_l ZRT}. \tag{7}$$

Due to the Boussinesq approximation, the continuity equation can be written in the following form:

$$\nabla \cdot \mathbf{v} = 0. \tag{8}$$

In bulk water, the Navier–Stokes equation is used to calculate velocity:

$$\rho\left(\frac{\partial \mathbf{v}}{\partial t} + \mathbf{v} \cdot \nabla \mathbf{v}\right) = -\nabla p + \mu \nabla^2 \mathbf{v} + \rho g. \tag{9}$$
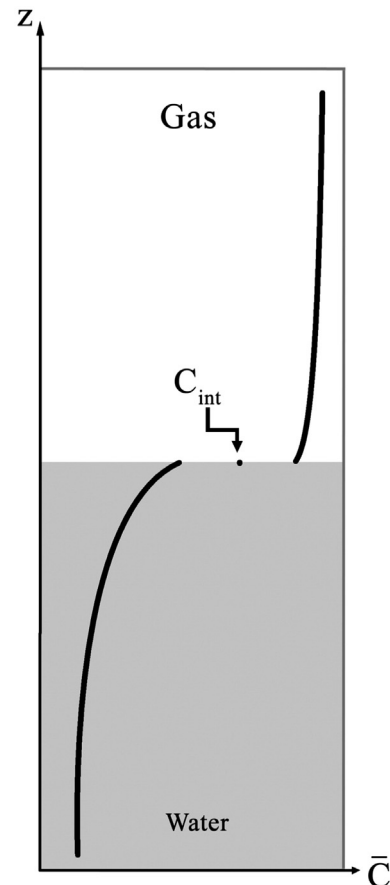

Fig. 3. Schematic profile of concentration versus height of cell.

The convection–diffusion equation is used for calculating the concentration:

$$\frac{\partial c}{\partial t} - \nabla \cdot (D\nabla c) + \mathbf{v} \cdot \nabla c = 0. \tag{10}$$

The boundary and initial conditions for the velocity and concentration equation i.e. Eqs. (9) and (10) are given in Tables 1 and 2. In Eq. (9), density of mixture is calculated using the following equation:

$$\rho = \frac{\rho_w}{1 - y_{CO_2} \left(1 - \frac{V_\varphi}{M_{CO_2}} \rho_w \right)}. \tag{11}$$

V_φ is the apparent volume of CO_2 (m³/mol) and can be calculated by the following equation [34]:

$$V_\varphi = 37.51 - 9.585 \times 10^{-2}T + 8.74 \times 10^{-4}T^2 - 5.044 \times 10^{-7}T^3 \tag{12}$$

where T is in °C and V_φ is in cm³/mol. For the case of our experiment (at $T = 30.5$ °C), V_φ is equal to 35.3853 cm³/mol.

Tharanivasan et al. [35] mentioned that there are three kinds of BCs in the gas–liquid interface representing three different interface mass transfer models:

$$C_{eq} = \frac{P_{eq} C_t}{K_h} \tag{13}$$

$$C = \frac{P(t) C_t}{K_h} \tag{14}$$

$$D\frac{\partial C}{\partial z}\Big]_{z=H} = k\left(C_{z=H} - C_{eq}\right). \tag{15}$$

These boundary conditions are known as: equilibrium, semi-equilibrium, and non-equilibrium, respectively. Tharanivasan et al. [35] used the experimental data of CO_2 and CH_4 dissolution in heavy oil from Zhang et al. [30], and suggested that different boundary conditions are required to model different systems. We will investigate these three types of boundary conditions for the CO_2–water system. First, these types are introduced:

(A) Equilibrium BC: From Henry's law,

$$K_h \frac{C}{C_t} = P \tag{16}$$

where C_t is the total concentration of CO_2 and water.
If we assume that pressure change along the test is not that much to have a significant effect on saturation concentration, the interface concentration can be calculated from the following equation at the initial pressure. We call this equilibrium BC:

$$C = \frac{C_t}{K_h} P_i \tag{17}$$

(B) Semi-equilibrium BC: By combining Eqs. (5) and (16),

$$K_h \frac{C}{C_t} = \left(\frac{-V_l ZRT \, \bar{c}_{CO_2}}{V_g} + P_i \right). \tag{18}$$
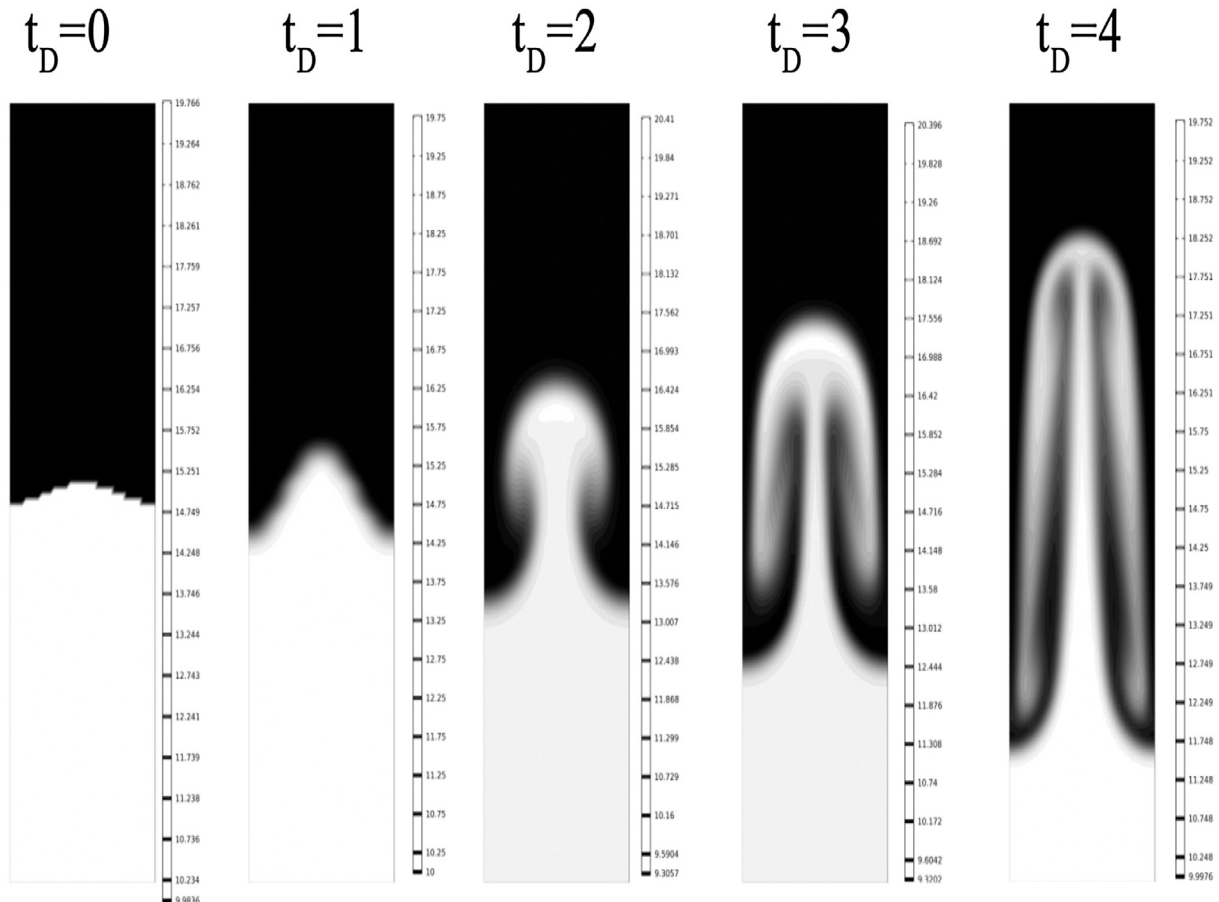

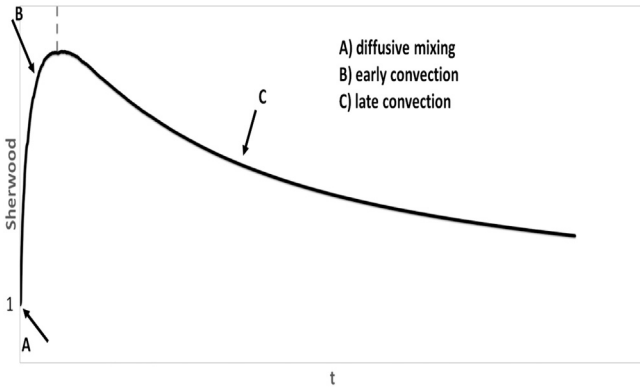Fig. 4. Temperature distribution for a miscible Rayleigh–Taylor problem; compare with Fig. 5 of [38].

Fig. 5. Dissolution sequences in bulk water denoted by Sherwood number.

Fig. 7. Profile of average concentration for convective and diffusive mixing.

Thus, concentration at the gas/liquid interface can be obtained by:

$$C = \frac{C_t}{K_h}\left(\frac{-V_l ZRT\,\bar{c}_{CO_2}}{V_g} + P_i\right).$$

(19)

We call it semi-equilibrium BC.

(C) Non-equilibrium BC: Etminal et al. [27] modeled the interface resistance and mentioned that mass transfer coefficient does not necessarily imply physical resistance. They used the following boundary condition representing resistance at the interface:

$$D\frac{\partial C}{\partial z}\Big|_{z=H} = k\left(C_{g\text{-}int}(t) - C_{z=H}\right)$$

(20)

where $C_{g\text{-}int}$ is the gas concentration above the interface and is time dependent and $C_{z=H}$ is gas concentration below the interface. It should be noted that the interface volume is zero and a sharp change exists at the interface. Gas concentration above the interface can be calculated from Henry's law:

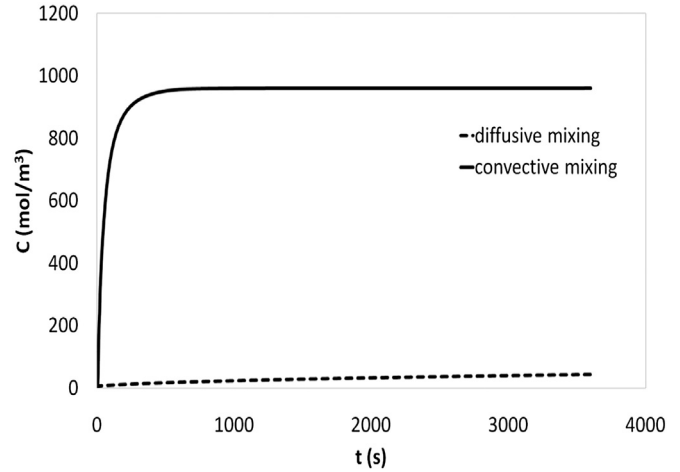$$C_{g\text{-}int}(t) = \frac{C_t}{K_h}P(t).$$

(21)

This boundary condition, as the authors stated, covers the whole equilibrium and non-equilibrium behaviors. We will refer to it as non-equilibrium BC, which prevents instantaneous equilibrium and there is a large difference between concentration below and above the interface especially at the start of tests when the gas pressure (and concentration above the interface) is maximum and flux is largest, as shown schematically in Fig. 3.

Using this BC makes the diffusion equation non-linear and thus, it is difficult to present an analytical solution for diffusion equation. Etminal et al. [27] gave the solution in Laplacian domain and used the Stehfest algorithm to find the inverse transform.

4. Numerical scheme

The modeling is performed in a geometry having the same dimensions and conditions of our experimental diffusion cell. The above mentioned problem is solved using the Finite Element Method (FEM). The physical domain is discretized into 51×20 quadrilateral linear elements. The grid refinement is in good agreement since finer grids had the same results.

The Navier–Stokes equations are solved using a projection method [36] in which a Poisson equation for pressure is derived and numerically
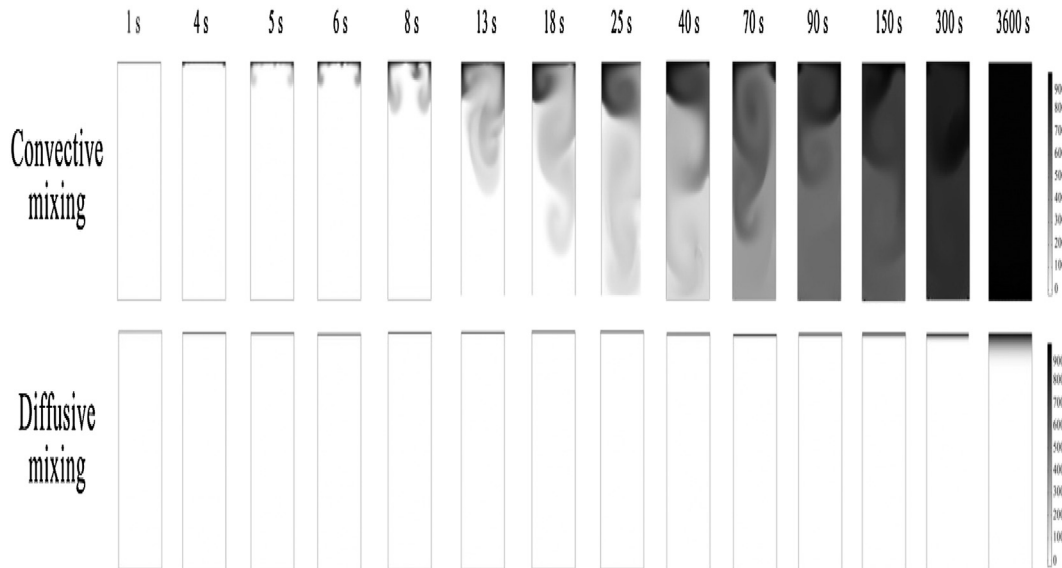

Fig. 6. Profile of CO_2 dissolved in water in mol/m³. There is a significant difference between convective and diffusive mixing.
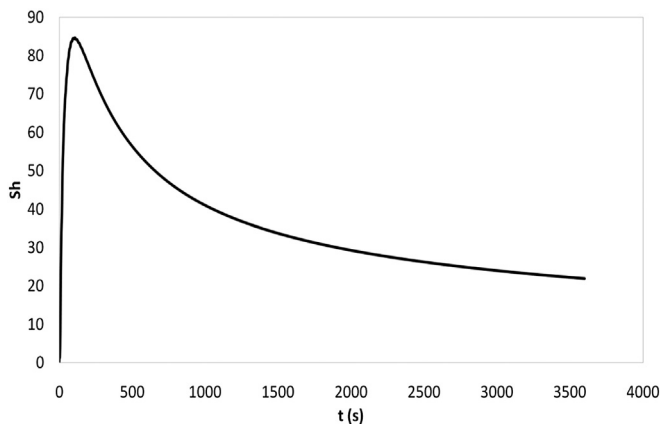
Fig. 8. The plot of Sherwood number versus time for the main simulation.

Fig. 10. Effect of different BCs on the pressure versus time data when $D = 4.5e-9$ m/s (the equilibrium BC, quasi-equilibrium BC and non-equilibrium BC with $k = 4.5e-3$ m/s are indicated versus experimental data).

solved. To prevent non-physical oscillations, the Streamline Upwind Petrov–Galerkin (SUPG) method and crosswind artificial diffusion is used [37]. The code is validated by solving a similar heat transfer problem in which a heavier fluid is brought on top of a lighter fluid. The result of temperature distribution can be found in Fig. 4. This figure can be compared to the original results given by Liu and Guo [38]. We have used the same parameters and information given in their paper and Fig. 4 of our results is according to Fig. 5 of their paper. For more details please see the reference.

5. Results and discussion

The equilibrium BC is used here for having a better comparison with previous works. So that we divide our results into two sub-sections: A) equilibrium mixing and B) comparison with experimental data. In the first section dissolution sequences are distinguished and dissolution with the presence of convection is compared to pure diffusive mixing. In the second section, the main concern is presenting a result compatible with experimental data. Therefore, three types of boundary conditions are used. Also, some experimental data and measurements are provided.

5.1. Equilibrium mixing

The dissolution of CO_2 in bulk water begins as the CO_2 diffuses across the interface. At the gas/liquid interface, CO_2 saturated water layer forms that is heavier than water and thus, it can sink to the bottom of cell. This heavier layer is immediately destabilized and convection triggers as an active mechanism.
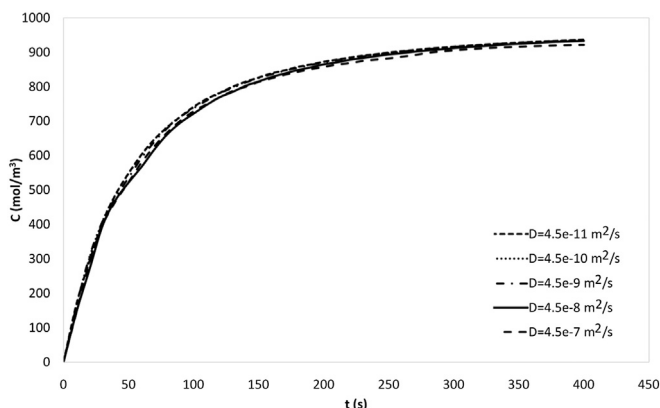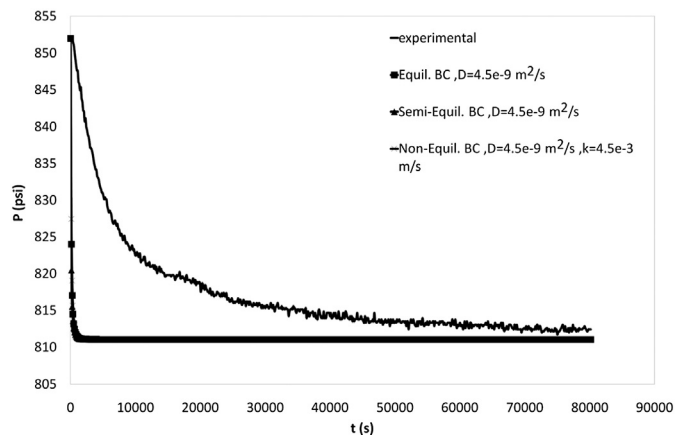
The scaling relationships of CO_2 dissolution in water are thoroughly explained by Hassanzadeh et al. [13] for a 2-D porous layer model. They showed that there are three periods of CO_2 mixing in water including: A) diffusive mixing, B) early convective mixing, and C) late convective mixing. These periods are shown schematically in Fig. 5 for dissolution in bulk water. Hassanzadeh et al. used the Sherwood number to characterize different steps of dissolution. The Sherwood number is defined as the ratio of total mixing to diffusive mixing and is calculated using the following equation.

$$Sh = \frac{\overline{C}\big)_{convective\ mixing}}{\overline{C}\big)_{diffusive\ mixing}} \qquad (22)$$

In bulk water, the first period (A) is usually too short that it cannot be observed. This is due to the fact that instability is quickly emerged and no baffle, or say solid grains of porous medium, is present to prevent convection growing unlike dissolution with the presence of a porous medium. The rate of dissolution at the period of early diffusion (A) is slow.

For systems that convection cannot develop (in low permeable porous media), this period continues and remains as the only dissolution mechanism. It is obvious that the Sherwood number is kept unity during this period.

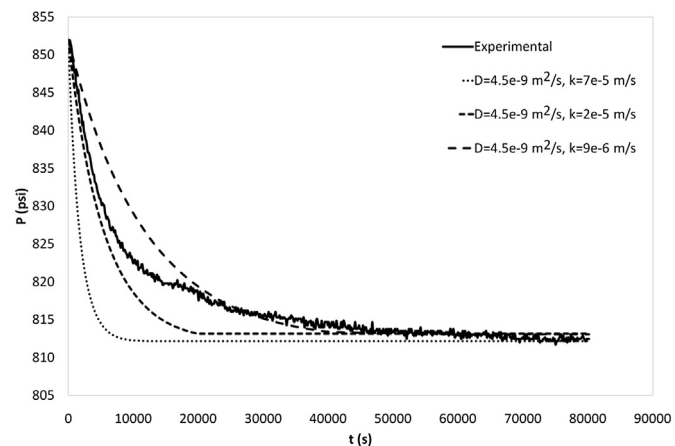Fig. 9. Equilibrium convective mixing for the first 400 s.

Fig. 11. The results of the model are compared to experimental data for different mass transfer coefficients while diffusion coefficient equals to $4.5e-9$ m^2/s.
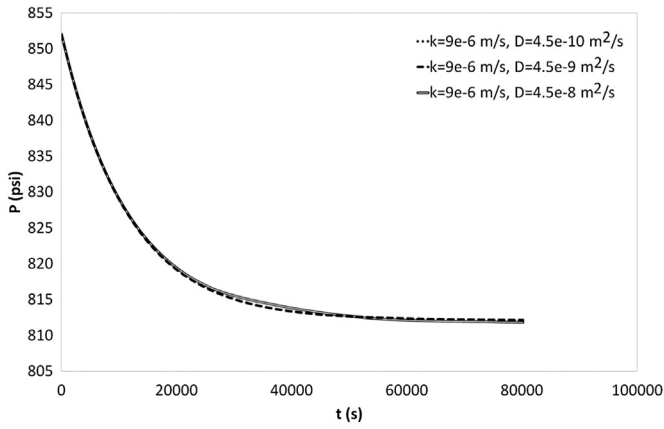
Fig. 12. Effect of different values of diffusion coefficient on non-equilibrium mixing when $k = 9e-6$ m/s.

The CO_2-saturated layer of water at the interface is unstable and convection begins immediately as the instabilities are growing. These instabilities are in the forms of micro fingers joining each other to form larger ones. Physical perturbation imposed by system vibrations and oscillations can help this process to develop.

As time passes, convection grows while fingers are developing (period B). At later times, especially when the fingers reach the bottom of the cell, a more uniform concentration of CO_2 is expected. Therefore, it can be concluded that the convection at later times (period C) is gradually weakened. Convective dissolution is controlled by the dimensionless Rayleigh number, defined as Eq. (23):

$$Ra = \frac{g\Delta\rho^* L^3}{\mu D} \tag{23}$$

where $\Delta\rho^*$ is the density difference between saturated water with CO_2 and pure water. In a porous medium, convection can grow for systems with the Rayleigh number higher than 40. For the Rayleigh number close to (and higher than) 40, convection slightly deviates the flat diffusive layer. Increasing the Rayleigh number results in developing fingers with smaller or more perturbed shapes. For the application of geological sequestration, the Rayleigh number hardly increases over the order of 1000. On the other hand, the order of this number is around 10^{11} based on Eq. (23) and the reported value of the diffusion coefficient for our system in bulk water in laboratory. The velocity in a porous medium is governed by Darcy's law. While, in bulk water the Navier–Stokes formulation determines the velocity caused by natural density

driven convection. Thus, these differences make the flow in bulk liquid more complex. A few simulation or modeling considers this problem in bulk liquid medium. We can see further that the scaling in bulk water needs a special consideration.

The modeling shows that dissolution due to density-driven convection is so faster than the pure diffusion, as shown in Fig. 6. From this figure, it can be observed that the short tail instabilities form at early times.

These are microscopic instabilities in the reality while after a short period of time (say a moment) they join each other and forms longer and wider instabilities, so that, they can be observed like the third panel for convective mixing at the time of 5 s. They continuously join each other and make larger fingers just like those at the 8 s panel. They finally emerge as plumes like the ones at the time of 70 s or 90 s, which are sunk to the bottom in a form similar to the Rayleigh–Taylor problem [12,39].

The profile of concentration in bulk liquid versus time for convective and diffusive mixing is plotted in Fig. 7. According to this figure, it takes almost 600 s to reach the water saturated with CO_2, while at the same time only 2.4% of CO_2 is dissolved under pure diffusion mechanism and becomes 4.57% at 3600 s. As it shows, the profile of convective mixing separates from diffusive mixing immediately.

This is due to the fact that onset of convection is too soon in bulk water to be observed discretely, while in porous media the term "onset of convection" is used for the beginning of convective mixing. Unlike the dissolution in the porous medium, there is no visible critical wavelength standing for the instability triggering density-driven convection in bulk liquid.

Once again a plot of the Sherwood number versus time is shown in Fig. 8 with a focus on its magnitude. It has the same trend as that observed by Hassanzadeh et al. [13] and shown in Fig. 5. However, the Sherwood number in our problem is an order of magnitude larger than them and it seems that the Sherwood number becomes equal to unity at infinite times.

The Sherwood number falls very slowly at late convection period. It shows that convection is the active mechanism even at late times. This phenomenon interferes with diffusivity measurements and makes results interpretation difficult both at early and later times. Once convection begins, it continues as the main mechanism of dissolution.

On the other hand, diffusive flux is the dominant mechanism when there is a concentration gradient along the liquid. At later times, the whole water column is almost saturated with CO_2 and thus it is impossible to find diffusivity at this period. In this case, a plot of concentration versus time (Fig. 9) shows the same profile for different diffusion coefficients from $4.5e-7$ m²/s to $4.5e-11$ m²/s, which corresponds to Rayleigh numbers between 2.86e8 and 2.86e12. Very little difference was observed between curves, which implies that equilibrium convective
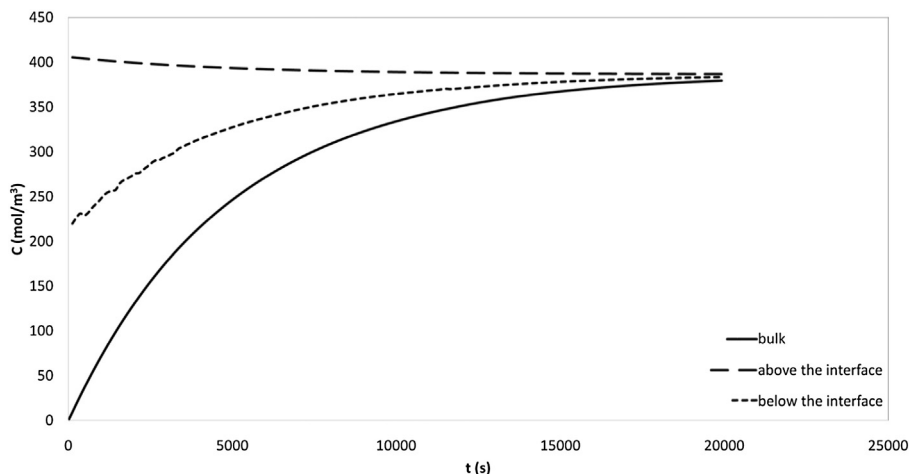

Fig. 13. Behavior of concentration above and below the interface and in bulk liquid versus time, $D = 4.5e-9$ m²/s, $k = 9e-6$ m/s (CO_2/water).

dissolution with high Rayleigh numbers is independent of the Rayleigh number itself.

In other words, diffusive flux is negligible when convective dissolution with large Rayleigh numbers happens. We know that diffusion is a slow mechanism. Our modeling showed that it took 6 days to have a saturated water column with CO_2 while it reduces to 18 h when convection is active. Fig. 9 shows simulated results for different diffusion coefficients while convection is active. It is plotted for the first 400 s, where the largest difference between cases is expected.

5.2. Comparison with experimental data

As mentioned before, the modeling is based on experimental procedure. Three boundary conditions are here used. Fig. 10 shows modeling results with different BCs. It is clear from this figure that equilibrium and quasi-equilibrium BCs have far deviation in early times compared to the experimental data. Also, non-equilibrium BC with high value of mass transfer coefficient ($k > 1e-3$ m/s) showed almost the same result as the equilibrium BC.

High values of k imply that there is no difference in concentration across the interface. Thus, equilibrium boundary condition may be considered as a special case of non-equilibrium, Robin type boundary condition. This point is well mentioned by Rasmussen and Civan [3] that in the case of higher mass transfer coefficient both non-equilibrium and equilibrium BC have the same results.

Results of simulations with different mass transfer coefficients on condition of non-equilibrium BC are plotted in Fig. 11 and compared with experimental measurements. The early and late time data is matched with $k = 2e-5$ m/s and with $k = 9e-6$ m/s, respectively. This value can be compared to the approximate value of $5.75e-5$ m/s obtained by Yang and Gu [40] for CO_2 in brine at $P = 522$ psi and $T = 25\ °C$.

According to this figure, early mass transfer coefficient is higher, implying a stronger convection at early times. Dependence of CO_2 dissolution to mass transfer coefficient is much stronger than the diffusion coefficient itself. Fig. 12 compares pressure decay results for three diffusion coefficients that differ an order of magnitude. According to this figure, diffusion coefficient does not change the pressure decay trend when non-equilibrium BC governs the whole process.

The change in bulk concentration and also above the interface and below the interface concentration is shown in Fig. 13.

The largest difference between concentration above and below the interface can be observed at the beginning and it decreases versus
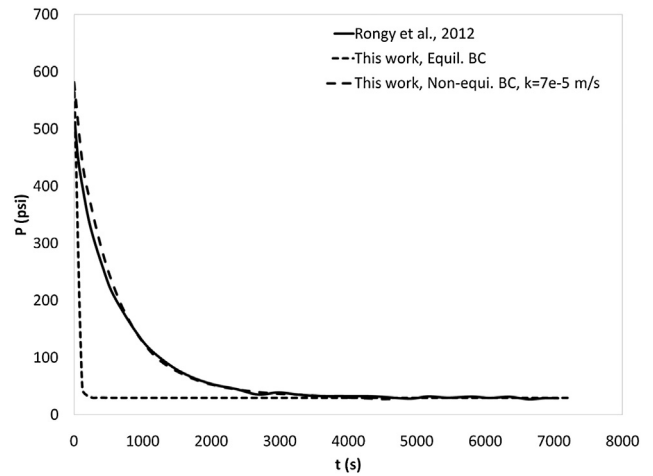
Fig. 15. The results of this work are compared to pressure–time data of Rongy et al. [28].

time. It shows that CO_2 mass flux reduces versus time since the liquid reaches a saturated mixture. All profiles are approaching to the equilibrium concentration. The effect of mass transfer coefficient on the Sherwood number in the case of non-equilibrium BC is shown in Fig. 14. It can be seen that the maximum Sherwood number increases and also happens earlier as mass transfer coefficient increases. In this manner two important scaling relationships were found to be valid for our results:

$$Sh_{max} = 0.54427 \left(\frac{t_{sh,max} D}{H^2} \right)^{-0.49096} \tag{24}$$

$$Sh_{max} = 0.9322 \left(\frac{kH}{D} \right)^{0.4026} \tag{25}$$

To validate our assumptions and modeling results, the problem of Rongy et al. has been followed [28]. They focused on modeling of CO_2 and CH_4 dissolution in n-C_{10}. Their problem is so similar to this work with some differences compared to what was mentioned in model section. They considered both phases and thus the effect of water evaporation and pressure gradient in gas phase was taken into account. Also, swelling of n-C_{10} due to dissolution and dependence of concentration on diffusion coefficient was considered as well.
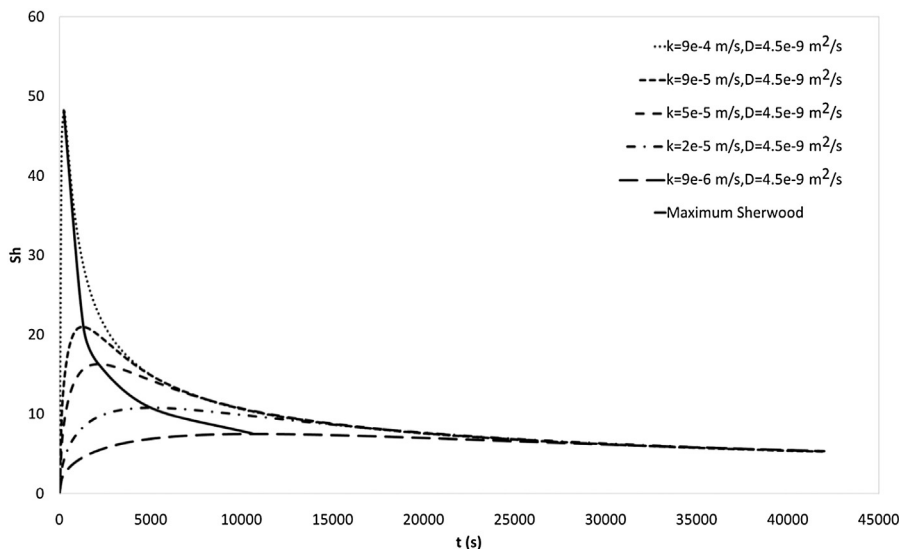
Fig. 14. Trend of Sherwood number versus time when different mass transfer coefficients are used.
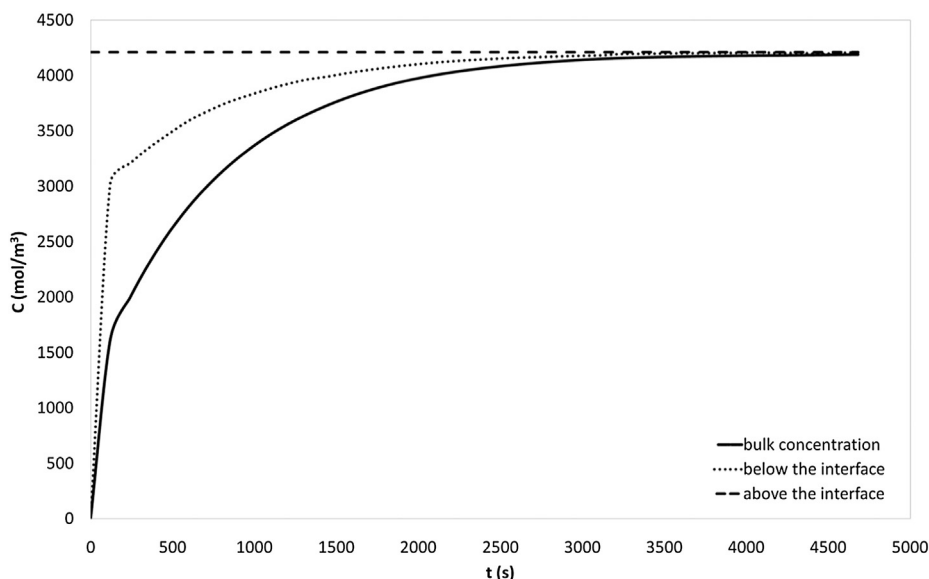
Fig. 16. Behavior of concentration above and below the interface and in bulk liquid versus time (CO_2/n-C_{10}).

The non-equilibrium BC used here assumes that concentration above the interface remains constant during the experiment and is calculated using Henry's law. It was found that simulated data with equilibrium boundary condition has a large discrepancy to their results at early times, as shown in Fig. 15.

According to this figure, the non-equilibrium BC with $k = 7e-5$ m/s gives almost the same results as the experiment measurements. For our simulation data, the value of $5.6e-9$ m^2/s used for diffusion coefficient as reported by Rongy et al. [28]. Our model fits the experimental data with one value of mass transfer coefficient at later times. Also, deviation at early times is noticeable in Fig. 16. Like the CO_2/water system, higher mass transfer coefficient at early time is observed.

A higher mass transfer coefficient implies a faster mass transfer across the interface. For the CO_2/n-C_{10} system, mass transfer across the interface is expected to be faster and more dominant than the CO_2–water system. Dissolution of CO_2 in water takes almost 65,000 s (18 h) to reach equilibrium, while this value is 4500 s (1.25 h) for CO_2/n-C_{10}. On the condition of $k = 7e-5$ m/s concentrations above and under the interface and in the bulk liquid are plotted in Fig. 16.

Fig. 17 shows the concentration contours of CO_2 weight fraction resulted from this work. Panels at the same times as Fig. 8 of Rongy et al. [28] are shown to be compared to their work. Disturbances in concentration profile can be observed at different times. Our results show that CO_2 tends to reach to the bottom layer by layer rather than fully perturbing system, as shown in panels at 174.5 s, 177.5 s and 179 s.
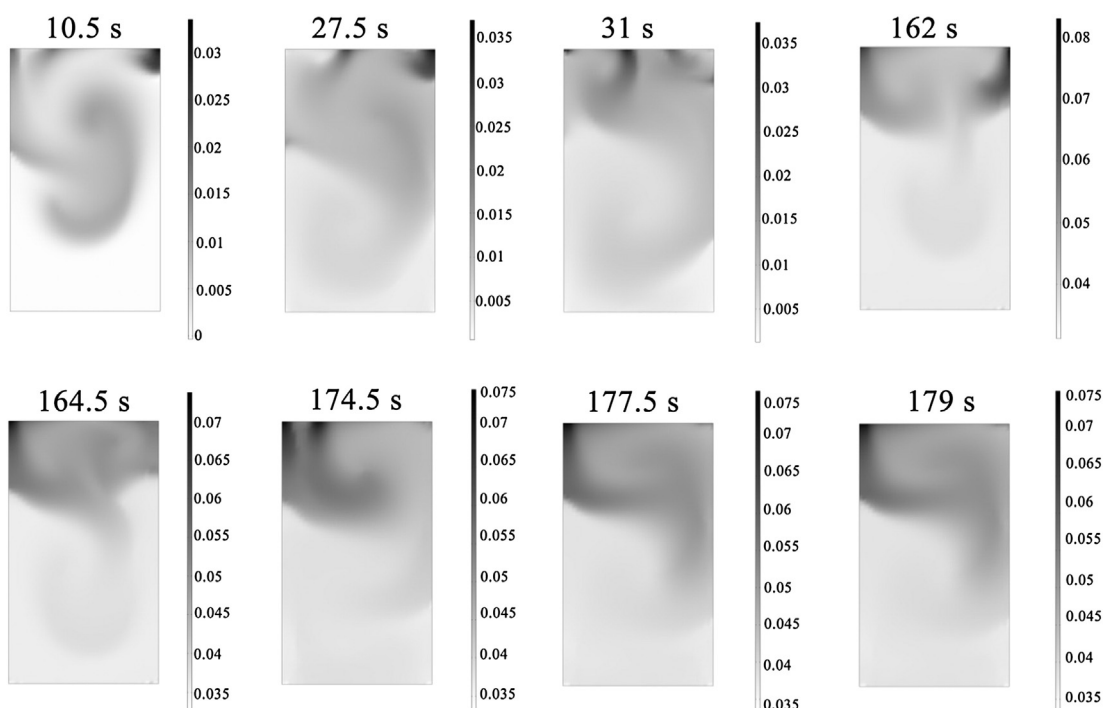

Fig. 17. Profile of concentration selected in the same times as Fig. 7 of Rongy et al. [28].

6. Conclusions and remarks

Dissolution of CO_2 in bulk water under different boundary conditions is simulated and the following conclusions are drawn:

1. Trend of the Sherwood number is similar to that observed in the presence of porous medium. However, its magnitude and duration of different periods are significantly different. In the case of equilibrium BC, the maximum Sherwood number is an order of magnitude higher than its value observed in porous media.
2. The Sherwood number is a function of mass transfer coefficient and there is a power relationship between the maximum Sherwood and mass transfer coefficient.
3. Comparing our modeling results with experimental data shows that non-equilibrium BC describes the behavior of dissolution well. Other BCs show considerable deviations.
4. A single mass transfer coefficient cannot predict dissolution behavior and its value decreases as dissolution goes by. For systems like $CO_2/n-C_{10}$ that reaches to equilibrium quickly, larger mass transfer coefficients are expected.
5. The effect of interface resistance should be taken into account for modeling. Models with lower mass transfer coefficients imply larger resistance and indicate lower Sherwood numbers.
6. Diffusive transport is insignificant when density driven convection is an active and dominant mechanism.
7. Dissolution is controlled by convective dissolution in bulk water where there is no obstacle or a porous medium to prevent convective swirls. Thus, to observe the effect of diffusive transport a special method is required. Presence of a porous medium is suggested to act as baffles or obstacles to prevent convection growing.
8. In order to use a method such as pressure decay to calculate diffusion coefficient, absence of fluid velocities is essential. The effect of natural density-driven convective dissolution in pressure reduction is like diffusive dissolution but much stronger.

Nomenclature

A	cell area (m^2)
c	concentration (mol/m^3)
D	diffusion coefficient (m^2/s)
g	gravity acceleration (m/s^2)
H	height of the liquid (m)
k	mass transfer coefficient (m/s)
K	constant
L	height of diffusion cell (m)
M	molar mass (g/mol)
n	mole
P	pressure (Pa or psi)
R	gas constant (Pa m^3/mol K)
Ra	Rayleigh number
Sh	Sherwood number
T	temperature (K)
u	x-component velocity (m/s)
v	y-component velocity (m/s)
$\mathbf{v}$	velocity vector (m/s)
y	weight fraction of dissolved CO_2
z	position along diffusion cell (m)
Z	gas compressibility factor
μ	viscosity (Pa s)
ρ	density (kg/m^3)

Subscript

eq	equilibrium
D	dimensionless
g	gas
H	Henry's constant
i	initial
int	interface
l	liquid
max	maximum
sat	saturated
t	total
w	water

References

[1] T. Ahmed, H. Nasrabadi, A. Firoozabadi, Complex flow and composition path in CO_2 injection schemes from density effects, Energy Fuel 26 (2012) 4590–4598.
[2] F. Civan, M.L. Rasmussen, Determination of gas diffusion and interface-mass transfer coefficients for quiescent reservoir liquids, SPE J. 11 (2006) (84072-PA).
[3] M.L. Rasmussen, F. Civan, Parameters of gas dissolution in liquids obtained by isothermal pressure decay, AIChE J. 55 (2009) 9–23.
[4] T. Loulou, B. Adhikari, D. Lecomte, Estimation of concentration-dependent diffusion coefficient in drying process from the space-averaged concentration versus time with experimental data, Chem. Eng. Sci. 61 (2006) 7185–7198.
[5] M. Jamialahmadi, M. Emadi, H. Müller-Steinhagen, Diffusion coefficients of methane in liquid hydrocarbons at high pressure and temperature, J. Pet. Sci. Eng. 53 (2006) 47–60.
[6] P. Drazin, Introduction to hydrodynamic instability, Cambridge Texts in Applied Mathematics, 2002.
[7] L. Rayleigh, XX. On the equilibrium of liquid conducting masses charged with electricity, The London, Edinburgh, and Dublin Philosophical Magazine and Journal of Science 14 (1882) 184–186.
[8] G. Taylor, in: Proc. Roy. Soc. Lond. 219 (1953) 186–203.
[9] H. Hele-Shaw, The flow of water, Nature 58 (1898) 34–36.
[10] L. Rayleigh, LIX. On convection currents in a horizontal layer of fluid, when the higher temperature is on the under side, Lond. Edinb. Dublin Philos. Mag. J. Sci. 32 (1916) 529–546.
[11] H. Bénard, Les tourbillons cellulaires dans une nappe liquide.-Méthodes optiques d'observation et d'enregistrement, J. Phys. Theor. Appl. 10 (1901) 254–266.
[12] P.G. Saffman, G. Taylor, The penetration of a fluid into a porous medium or Hele-Shaw cell containing a more viscous liquid, Proc. R. Soc. Lond. A Math. Phys. Sci. 245 (1958) 312–329.
[13] H. Hassanzadeh, M. Pooladi-Darvish, D.W. Keith, Scaling behavior of convective mixing, with application to geological storage of CO_2, AIChE J. 53 (2007) 1121–1131.
[14] K. Ghesmat, H. Hassanzadeh, J. Abedi, The effect of anisotropic dispersion on the convective mixing in long-term CO_2 storage in saline aquifers, Fluid Mech. Transp. Phenom. 57 (2011) 561–570.
[15] H.M. Ouakad, H. Nasrabadi, Onset of convection and advection in the CO_2 sequestration problem using the lattice Boltzmann method, Int. J. Adv. Sci. Eng. Technol. 2 (2012) 68–75.
[16] M. Szulczewski, M. Hesse, R. Juanes, Carbon dioxide dissolution in structural and stratigraphic traps, J. Fluid Mech. 736 (2013) 287–315.
[17] R. Farajzadeh, P.L. Zitha, J. Bruining, Enhanced mass transfer of CO_2 into water: experiment and modeling, Ind. Eng. Chem. Res. 48 (2009) 6423–6431.
[18] K.B. Haugen, A. Firoozabadi, Mixing of two binary nonequilibrium phases in one dimension, AIChE J. 55 (2009) 1930–1936.
[19] M.R. Riazi, A new method for experimental measurement of diffusion coefficients in reservoir fluids, J. Pet. Sci. Eng. 14 (1996) 235–250.
[20] S.R. Etminan, B.B. Maini, Z. Chen, H. Hassanzadeh, Constant-pressure technique for gas diffusivity and solubility measurements in heavy oil and bitumen, Energy Fuel 24 (2010) 533–549.
[21] E. Behzadfar, S.G. Hatzikiriakos, Diffusivity of CO_2 in bitumen: pressure-decay measurements coupled with rheometry, Energy Fuel 28 (2014) 1304–1311.
[22] R.N. Moghaddam, B. Rostami, P. Pourafshary, Y. Fallahzadeh, Quantification of density-driven natural convection for dissolution mechanism in CO_2 sequestration, Transp. Porous Media 92 (2012) 439–456.
[23] H. Sheikha, A.K. Mehrotra, M. Pooladi-Darvish, An inverse solution methodology for estimating the diffusion coefficient of gases in Athabasca bitumen from pressure-decay data, J. Pet. Sci. Eng. 53 (2006) 189–202.
[24] H. Sheikha, M. Pooladi-Darvish, A.K. Mehrotra, Development of graphical methods for estimating the diffusivity coefficient of gases in bitumen from pressure-decay data, Energy Fuel 19 (2005) 2041–2049.
[25] S.M. Ghaderi, S.H. Tabatabaie, H. Hassanzadeh, M. Pooladi-Darvish, Estimation of concentration-dependent diffusion coefficient in pressure-decay experiment of heavy oils and bitumen, Fluid Phase Equilib. 305 (2011) 132–144.
[26] F. Civan, M.L. Rasmussen, Improved Measurement of Gas Diffusivity for Miscible Gas Flooding Under Nonequilibrium vs. Equilibrium Conditions, 2002.

[27] S. Reza Etminan, M. Pooladi-Darvish, B.B. Maini, Z. Chen, Modeling the interface resistance in low soluble gaseous solvents–heavy oil systems, Fuel 105 (2013) 672–687.
[28] L. Rongy, K.B. Haugen, A. Firoozabadi, Mixing from Fickian diffusion and natural convection in binary non-equilibrium fluid phases, AIChE J. 58 (2012) 1336–1345.
[29] R. Azin, M. Mahmoudy, S.M. Jafari Raad, S. Osfouri, Measurement and modeling of CO_2 diffusion coefficient in saline aquifer at reservoir conditions, Cent. Eur. J. Eng. 3 (2013) 585–594.
[30] Y.P. Zhang, C.L. Hyndman, B.B. Maini, Measurement of gas diffusivity in heavy oils, J. Pet. Sci. Eng. 25 (2000) 37–47.
[31] E. Zamanian, M. Hemmati, M.S. Beiranvand, Determination of gas-diffusion and interface-mass-transfer coefficients in fracture-heavy oil saturated porous matrix system, Nafta 63 (2012) 351–358.
[32] M. Riazi, Pore Scale Mechanisms of Carbonated Water Injection in Oil Reservoirs. (PhD thesis dissertation thesis) Heriot-Watt University, 2011.
[33] R. Farajzadeh, P.L.J. Zitha, J. Bruining, Enhanced mass transfer of CO_2 into water: experiment and modeling, Ind. Eng. Chem. Res. 48 (2009) 6423–6431.
[34] J.E. Garcia, Density of Aqueous Solutions of CO_2, Lawrence Berkeley National Laboratory, 2001.
[35] A.K. Tharanivasan, C. Yang, Y. Gu, Comparison of three different interface mass transfer models used in the experimental measurement of solvent diffusivity in heavy oil, Pet. Sci. Eng. 44 (2004) 269–282.
[36] J. Guermond, P. Minev, J. Shen, An overview of projection methods for incompressible flows, Comput. Methods Appl. Mech. Eng. 195 (2006) 6011–6045.
[37] O. Zienckiewicz, R. Taylor, P. Nithiarasu, Elsevier Butterworth-Heinemann, Oxford, 2005.
[38] G. Liu, Z. Guo, Effects of Prandtl number on mixing process in miscible Rayleigh–Taylor instability: a lattice Boltzmann study, Int. J. Numer. Methods Heat Fluid Flow 23 (2013) 176–188.
[39] K. Ghesmat, Interfacial Instability of Reactive and Anisotropic Dispersive Miscible Flow Displacements(PhD thesis) University of Calgary, 2008.
[40] C. Yang, Y. Gu, A new method for measuring solvent diffusivity in heavy oil by dynamic pendant drop shape analysis (DPDSA), 112006. 48–57 (SPE 84202-PA).